Optimum design for buckling of arbitrary shaped ribs under uncertain loadings

A. C. Conrado, A. R. de Faria and S. F. M. de Almeida
Instituto Tecnológico de Aeronáutica,
São José dos Campos, Brazil

ABSTRACT

Typically, aircraft wing structural panels are designed against buckling for a very large number of possible loadings that may occur during the operation of the aircraft. If the optimisation procedure accounts only for a limited number of design loads, the structure may be vulnerable to a specific type of loading that may cause the structure to fail. A novel approach for the optimisation of ribs or plates of arbitrary shapes under uncertain loads is proposed. The geometry of the rib is defined by a single closed spline or several connected splines. The loading distribution is not considered to be uniform but it is allowed to vary within an admissible set, conferring uncertainty to the applied loads. The admissible load space comprises distributed normal and shear loadings that can be represented through a collection of piecewise linear functions defined along the plate boundary. A special procedure is applied to handle the constraint that the loading must be self equilibrating. A minimax strategy is used to deal with the loading variability such that the resulting optimal design is able to withstand an entire class of linear piecewise loadings along the rib boundary. The refinement of the loading representation may be completely independent of the refinement of finite element mesh. The validity of the proposed approach is assessed by applying it to an aeronautical wing rib.

NOMENCLATURE

$\mathbf{a}_i$, $\mathbf{b}_i$, $\mathbf{c}_i$, $\mathbf{d}_i$	spline coefficients
f_x , f_y	distributed loading components
G	matrix of the loading contribution of load control points to the equilibrium conditions
h	vector of thicknesses
I	identity matrix
l_{ij}	length between two points i and j over the spline
$\mathbf{n_i}$	unit vector
$\mathbf{p}_i$	spline knot coordinates
$\mathbf{q}_i$	co-ordinates of a point on the ith spline
R_i	uncertain loading components
r	vector of uncertain loadings
s	arc length parameter
$\mathbf{s}_i$	second derivative at point $\mathbf{p}_i$
w_i	weight with respect to load control point i
x, y	Cartesian coordinates
x	vector of load components for the load control points
y	vector of load components for the control points
Z	matrix of the loading contribution of spline control points to the equilibrium conditions
ϕ	solution of the inner loop of the minimax problem
λ	buckling load magnitude
Ψ	matrix of weights

1.0 INTRODUCTION

In most investigations conducted in the past addressing buckling optimisation of plates[1-5], the distribution of the applied loading remains fixed and uniform during the optimisation procedure such that the load magnitude is the parameter to be maximised[6]. For instance, when plates subjected to biaxial loads are studied, a constant load ratio is considered as a relation between the normal loads along each axis whose distributions are uniform.

Dealing almost exclusively with rectangular plates uniformly loaded, tables and diagrams are available in the literature[7,8] and still

Paper No. 2975. Manuscript received 18 April 2005, accepted 24 July 2005.

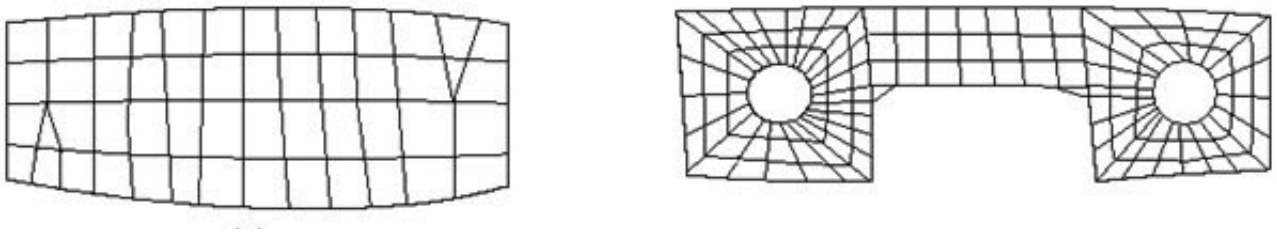

Figure 1. Typical mesh representation of ribs.

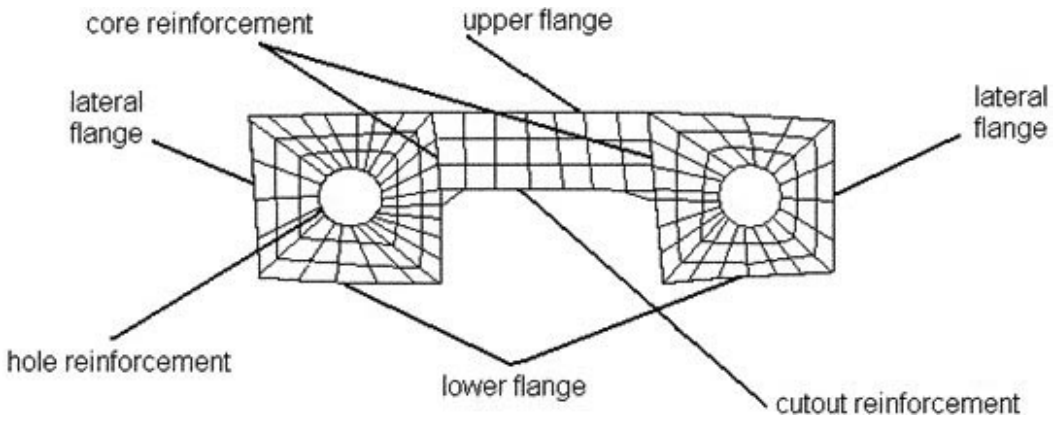

Figure 2. Rib flanges and reinforcements.

widely used by aircraft structural designers. However, perfectly uniform loading and rectangular plates are highly unlikely in practical applications. Ribs, skin panels and control surfaces constitute irregular geometries subjected to shear and normal loadings applied along its edges that are non-uniformly distributed. Moreover, typical structural components are often subjected to different load cases, most of them unlikely to be uniformly distributed.

Due to the potential sensitivity of optimal designs to loading variations, it is not conservative to consider uniform loading unless significant margins of safety are used in order to increase reliability. As a result, the designs are not optimal and may be heavier than required because of the loading uncertainty.

Novel approaches for optimising aircraft structural components should be able to deal with the multiplicity of the loading cases typically involved in actual designs. Innovative optimisation problems should be formulated to produce robust optimal designs that satisfy all possible loading cases to which the structure may be subjected. The new proposals must be computationally efficient in order to avoid unreasonably large computational models that cannot be handled by the currently available algorithms.

The objective of this work is to propose a design methodology that leads to optimised structures under uncertain loads. This methodology is quite general and employs a minimax optimisation strategy where the design variables are parameters that define the plate dimensions, and an arbitrarily piecewise linear mechanical loading distribution is considered. The loading discretisation makes it possible to deal with any boundary conditions and any loadings whereas the 2D geometry of the structure is completely arbitrary.

Ribs are employed in the construction of primary structural components such as wings, stabilisers, rudders or general control surfaces to provide torsional stiffness. Figure 1(a) illustrates a rib without cutouts and Fig. 1(b) presents a rib with typical cutouts and holes. The ribs usually have holes for different reasons such as passage for fuel lines, electric and electronic system cables, weight reduction, etc. A difficulty inherent to rib design, combined with the large number of the load cases involved, is the precise determination of the load transfer mechanism from skin panels and spars to the ribs. Figure 2 shows a rib with one cutout and two holes. Upper and lower flanges are in contact with the upper and lower skin panels, respectively. Lateral flanges are in contact with spars. Hence, the load transference will be through these interfaces, resulting in a self equilibrating system of loads applied to the rib (the rib is assumed to be in static equilibrium).

For the optimisation procedure proposed, the ribs are divided into several panels. These panels are defined by reinforcements and flanges. Figure 3 shows a rib divided into six panels.

The basic idea in the procedure proposed is to optimise ribs against an entire loading space rather than individual load cases one at a time. The loading space must be judiciously chosen in order to encompass all possible load cases and to take into account the load transfer mechanisms and possible special features of the rib under consideration such as stress concentration points, reinforcements and cutouts.

The loading space used in the present investigation is spanned by a series of piecewise linear basis functions defined on the rib boundary at selected points. If larger loading spaces are considered, the number of basis functions must be increased. This would burden the numerical procedures but ultimately renders the optimal ribs obtained more robust and less sensitive in the sense that more load cases or more load transferring mechanisms due to a variety of aircraft maneuvers will not result in buckling.

Once the rib (or any other structural component) as well as its applied loads are defined, the dimensions of each of these components can be optimised taking simultaneously all of the loading cases

https://doi.org/10.1017/S0001924000000944 Published online by Cambridge University Press

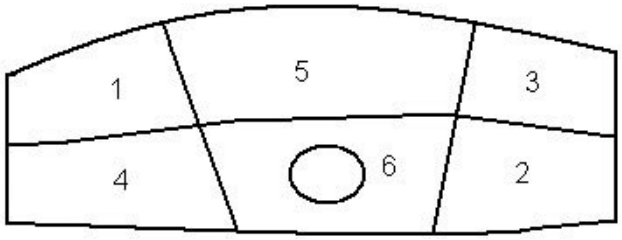

Figure 3. Rib panels.

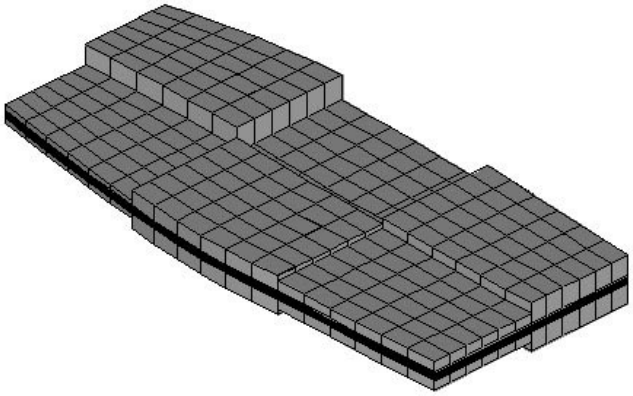

Figure 4. Piecewise constant thickness plate.

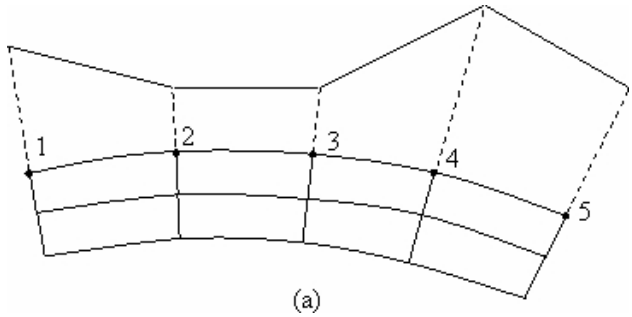

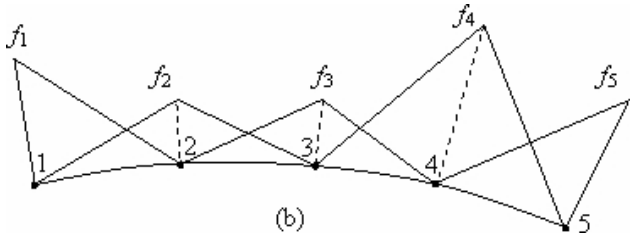

Figure 5. Discretisation of the loading distribution.

into account. Firstly, the rib is optimised considering each load case fixed and individually one at a time. Secondly, the optimisation is accomplished against the entire loading space.

The fundamental idea of this work is to propose an optimisation procedure that accounts for variations of the mechanical loading applied to arbitrary shaped plates. It is assumed that its distribution is arbitrarily piecewise linear and, therefore, uncertain or not fixed. The design obtained by the optimisation proposed is then compared with the others, optimised against only one load case, to show how it becomes insensitive to perturbations in the loading distributions within the admissible load set. A detailed explanation of the technique will be given for the construction of the whole admissible load set. As the basis linear piecewise functions are defined, three equilibrium equations can be used to generate a matrix with all independent loading distributions.

2.0 THE OPTIMISATION PROCEDURE

The design variables of the optimisation problem are the plate (or rib) thickness, the cross sectional (assumed rectangular) dimensions of reinforcements and the load distribution that varies continuously whereas the objective function is the critical buckling load. The objective function is calculated based on a classical linear prebuckling state and a linearised buckling problem. Furthermore, the plate is free of initial imperfections and simply supported along all edges. Details of the problem formulation can be found elsewhere[9-11].

The different thicknesses in the plate are illustrated in Fig. 4. In the middle of the plate there is a base plate such that at any point it defines the minimum thickness of the plate. The base plate thickness is kept constant during the optimisation procedure.

The general loading distributions are assumed to be piecewise linear and applied to the plates' edges as illustrated in Fig. 5. The basis piecewise linear functions are defined at five points 1, 2, 3, 4 and 5 in Fig. 5(a). A suitable choice of the heights f_1, f_2, f_3, f_4 and f_5 in Fig. 5(b) reflects the loading in Fig. 5(a). Points 1, 2, 3, 4 and 5 do not necessarily coincide with the nodes of the finite element mesh, but coincidence, as shown in Fig. 5a, facilitates the numerical procedures.

The optimisation problem must be formulated as to take into account the variability of the loading distribution. This can be done via a minimax formulation as given in Equation (1)[9-11]:

$$\max_{\mathbf{h}} \min_{\mathbf{r}} \lambda(\mathbf{h},\mathbf{r}) = \max_{\mathbf{h}} \phi(\mathbf{h}), \quad \phi(\mathbf{h}) = \min_{\mathbf{r}} \lambda(\mathbf{h},\mathbf{r}) \qquad \ldots (1)$$

where **h** is the vector of thicknesses and reinforcement dimensions, **r** is the vector of uncertain loads and λ is the buckling load magnitude, i.e. the objective function of the problem. The definition of **r** and the physical significance of its components R_i will be clarified in the next section. A constant mass constraint is also imposed.

The solution of the problem stated in Equation (1) provides, simultaneously, the optimal design and the worst loading combination in terms of **r**. The considered optimisation problem is bilevel and its numerical solution is often laborious. However, the fact that is obtained through solution of the classic eigenvalue problem allows for a tremendous simplification if the extended stability boundary theorem[9] is used. The bilevel optimisation problem in Equation (1) can be reduced to a classical optimisation problem where the objective function is evaluated by checking the buckling load λ associated with every individual loading basis function (Fig. 5) and selecting the minimum (worst) among them. This is how function $\phi(h)$ in Equation (1) is computed.

The overall optimisation problem is solved in two steps. The best design among randomly generated designs is taken as starting point for a Powell's search[12]. The use of Powell's method in this case is desirable because it is simple and avoids the complications caused by derivatives of possible repeated eigenvalues since gradients of the objective function are not required by the method. The optimisation stops when the relative difference between the previous and present values of ϕ does not exceed 0·001, where ϕ is the minimum λ over the admissible loading configurations.

https://doi.org/10.1017/S0001924000000944 Published online by Cambridge University Press

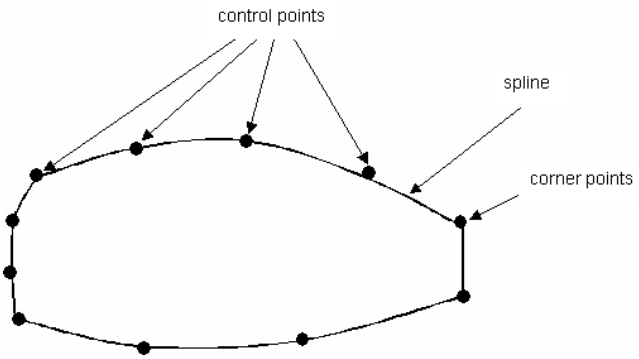

Figure 6. Rib-like geometry.

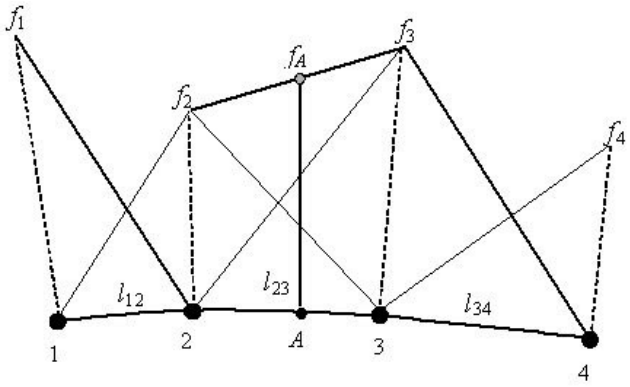

Figure 7. Load interpolation.

3.0 LOADING DISCRETISATION

The geometry of the plate or rib is described by an arbitrary number of concatenated splines defining a closed curve, as shown in Fig. 6. Each spline is defined by an arbitrary number of control points. A parametric cubic is defined between every two consecutive control points resulting in a continuous and smooth curve. Since a spline is always a smooth curve, corners are represented connecting two splines at a given point: the corner points shown in Fig. 6. In this case, there are two coinciding control points at the corner, each one belonging to one of the splines.

The spline parameters are computed based on the solution developed in Ref. 13. In each interval, between any two control points, a new cubic is used. The cubic spline must pass through all its control points and it is required that both the slope and the curvature be the same for the pair of cubics that share each control point. For the *i*th interval, between two consecutive control points the equations are:

$$\mathbf{q_i}(s) = \begin{Bmatrix} x_i(s) \\ y_i(s) \end{Bmatrix} = \mathbf{a_i}s^3 + \mathbf{b_i}s^2 + \mathbf{c_i}s + \mathbf{d_i} \qquad \ldots (2)$$

where the space coordinates x_i and y_i are cubic functions of the parameter s, that varies in the interval [0,1] between the two control points. $\mathbf{a_i}$, $\mathbf{b_i}$, $\mathbf{c_i}$ and $\mathbf{d_i}$ are 2×1 coefficient vectors. Let $\mathbf{s_i}$ be the second derivative at point $\mathbf{p_i}$. Then the coefficients in Equation (2) are calculated from the following equations[13]:

$$\mathbf{a_i} = \frac{\mathbf{s}_{i+1} - \mathbf{s}_i}{6} \qquad \ldots (3)$$

$$\mathbf{b_i} = \frac{\mathbf{s}_i}{2} \qquad \ldots (4)$$

$$\mathbf{c_i} = \mathbf{p}_{i+1} - \mathbf{p}_i - \frac{\mathbf{s}_1 + 2\mathbf{s}_{i-1}}{6} \qquad \ldots (5)$$

$$\mathbf{d_i} = \mathbf{p}_i \qquad \ldots (6)$$

The load distribution is discretised according to the procedure illustrated in Fig. 5. An arbitrary number of load control points are defined on each spline. In order to facilitate the formulation, the load control points are assumed to be a sub-set of the control points that define the spline. That is, not all points defining the spline are taken as load control points. However, it should be noticed that the first and last control points of each spline must be chosen as load control points.

Each load control point is associated with the magnitude of two load components, namely, the x and y components (f_x and f_y, respectively). Therefore, there are two load parameters for each load control point. Because there are two coinciding load control points at each corner, each corner is associated with four load parameters. Notice that splines joining at a given corner have different tangential and normal directions at this point.

The values of both the x and y components at an arbitrary point A over a curve, as in Fig. 7, is an interpolation of the values of the respective load components (f_2 and f_3) at the two neighboring load control points, points 2 and 3. The weights used in the interpolation are proportional to the distances to the load control points measured along the curves, such that the sum of the weights is always equal to 1. If the length from the point A to the nearest load control point in the left, point 2, is l_{2A} and the length to the nearest load control point in the right, point 3, is l_{A3}, then the weights are, respectively,

$$w_2 = \frac{l_{A3}}{l_{A3} + l_{2A}} \qquad \ldots (7)$$

$$w_3 = \frac{l_{2A}}{l_{A3} + l_{2A}} \qquad \ldots (8)$$

where $l_{2A} + l_{A3}$ is equal to the length l_{23} in Fig. 7. Therefore, the value of the load component f_A would be given by the Equation (9)

$$f_A = w_2 f_2 + w_3 f_3 \qquad \ldots (9)$$

where f_2 and f_3 are the load component at points 2 and 3, respectively.

In Fig. 7, point A is an arbitrary point over the spline, but is not a load control point. Points 1, 2, 3 and 4 are load control points as well as spline knots. Then the length between points 2 and A and the length between points A and 3 are

$$l_{2A} = \int_0^1 \sqrt{\left[\frac{\mathrm{d}x_i}{\mathrm{d}s}(s)\right]^2 + \left[\frac{\mathrm{d}y_i}{\mathrm{d}s}(s)\right]^2}\,\mathrm{d}s \qquad \ldots (10)$$

$$l_{A3} = \int_0^1 \sqrt{\left[\frac{\mathrm{d}x_{i+1}}{\mathrm{d}s}(s)\right]^2 + \left[\frac{\mathrm{d}y_{i+1}}{\mathrm{d}s}(s)\right]^2}\,\mathrm{d}s \qquad \ldots (11)$$

where i is the cubic curve between points 2 and A. If there were more control points between points 2 and A, or between points A and 3, the lengths in Equations (10) and (11) would be the sum of the consecutive cubic curve lengths.

https://doi.org/10.1017/S0001924000000944 Published online by Cambridge University Press

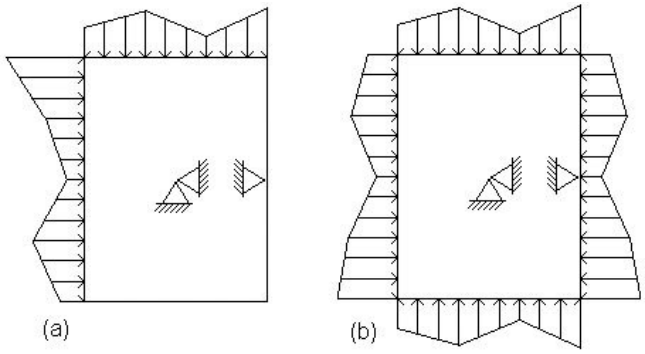

Figure 8. Plates under loads.

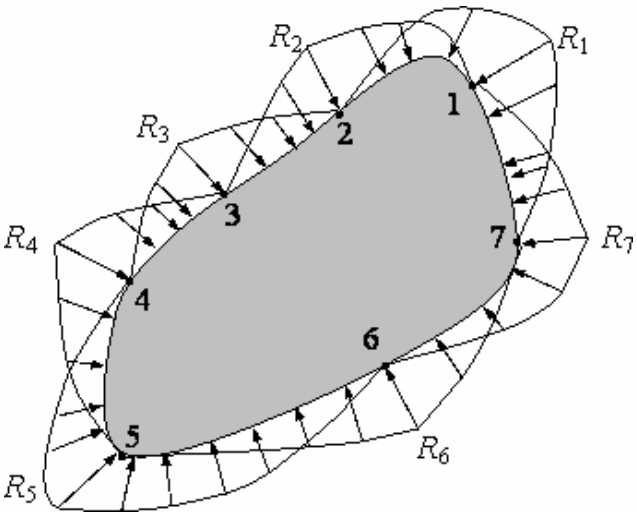

Figure 9. Loading discretisation.

4.0 SELF EQUILIBRATING CONDITION

To solve a buckling problem it is necessary to establish constraints to avoid rigid body movement. The position of these constraints should not affect the buckling modes. In Fig. 8(a) the plate is under a loading distribution that is not self-equilibrating and in Fig. 8(b) the distribution is self-equilibrating. It is clear that the buckling modes resulting from the plate in Fig. 8(a) are affected by the position of the constraints whereas, for the loading in Fig. 8(b), it does not happen since the boundary conditions are there just to prevent in-plane rigid body motion. Moreover, the load distribution applied by the wing components to the ribs must be self equilibrating.

Figure 9 illustrates an arbitrary set of distributed loadings applied along the boundary of an arbitrary shaped plate. Those loadings are defined at specific locations (load control points) and vary linearly such that the set of loadings comprises actually a set of piecewise linear distributed loadings. For instance, loading R_3 decreases linearly from point 3 to points 2 and 4 where it reaches zero. In Fig. 9 only normal distributed loadings are represented but it is also possible to define distributed shear loadings along the plate boundary in a similar manner. Alternatively, x and y Cartesian components may be used as in the following sections.

The distributed loading magnitudes are specified by the loading parameters R_i. However, if only self-equilibrating sets of loadings are admitted, then any combination of R_i's is generally not allowed.

Since the force and moment equilibrium conditions must be satisfied, there are three linear relations involving the loading parameters that must be satisfied:

$$\sum F_x = 0 \qquad \sum F_y = 0 \qquad \sum M_0 = 0 \qquad \ldots (12)$$

In order to cast Equation (12) in terms of the loading parameters, it is necessary to compute the contribution of the loading distribution associated to each individual load control point to the force components x and y and the moment about an arbitrary fixed point, taken as the origin of the xy coordinate system. The equilibrium equations in Equation (12) may be rewritten in terms of the force components f_{xi} and f_{yi} for each control point i:

$$\sum_i (I_i + J_i) f_{xi} = 0 \qquad \ldots (13)$$

$$\sum_i (K_i + L_i) f_{yi} = 0 \qquad \ldots (14)$$

$$\sum_i \left[-(N_i + O_i) f_{xi} + (T_i + U_i) f_{yi} \right] = 0 \qquad \ldots (15)$$

where the terms I_i, J_i, K_i, L_i, N_i, O_i, T_i and U_i represent the contribution of the loading distribution and are calculated as follows:

$$K_i = I_i = \int_0^1 s \sqrt{\left[\frac{dx_{i-1}}{ds}(s)\right]^2 + \left[\frac{dy_{i-1}}{ds}(s)\right]^2}\, ds \qquad \ldots (16)$$

$$L_i = J_i = \int_0^1 (1-s) \sqrt{\left[\frac{dx_i}{ds}(s)\right]^2 + \left[\frac{dy_i}{ds}(s)\right]^2}\, ds \qquad \ldots (17)$$

$$N_i = \int_0^1 s\left[y_{i-1}(s)\right] \sqrt{\left[\frac{dx_{i-1}}{ds}(s)\right]^2 + \left[\frac{dy_{i-1}}{ds}(s)\right]^2}\, ds \qquad \ldots (18)$$

$$O_i = \int_0^1 (1-s)\left[y_i(s)\right] \sqrt{\left[\frac{dx_i}{ds}(s)\right]^2 + \left[\frac{dy_i}{ds}(s)\right]^2}\, ds \qquad \ldots (19)$$

$$T_i = \int_0^1 s\left[x_{i-1}(s)\right] \sqrt{\left[\frac{dx_{i-1}}{ds}(s)\right]^2 + \left[\frac{dy_{i-1}}{ds}(s)\right]^2}\, ds \qquad \ldots (20)$$

$$U_i = \int_0^1 (1-s)\left[x_i(s)\right] \sqrt{\left[\frac{dx_i}{ds}(s)\right]^2 + \left[\frac{dy_i}{ds}(s)\right]^2}\, ds \qquad \ldots (21)$$

If the load control point is a corner point, some of the terms I_i, J_i, K_i, L_i, N_i, O_i, T_i and U_i will be zero and the point will appear twice in the equilibrium conditions, because it belongs to two splines. All integrals in the work are evaluated with ten-point Gaussian quadrature.

Adding the contributions of all loading parameters in the equilibrium equations in Equation (12) for the load control points yields:

$$\mathbf{G}\,\mathbf{x} = 0, \qquad \ldots (22)$$

where $\mathbf{G}$ is a $3 \times n$ matrix and $\mathbf{x}$ is a $n \times 1$ vector. The three rows in matrix $\mathbf{G}$ are the force and moment equilibrium conditions in Equation (12). The number of columns n in matrix $\mathbf{G}$ is twice the number of load control points because there are x and y load components to each point. The vector $\mathbf{x}$ has the load components for the load control points:

$$\mathbf{x}^T = \left\{ f_{x1} \quad f_{y1} \quad \ldots \quad f_{xi} \quad f_{yi} \quad \ldots \quad f_{xm} \quad f_{ym} \right\} \qquad \ldots (23)$$

https://doi.org/10.1017/S0001924000000944 Published online by Cambridge University Press

where $m = n / 2$.

In the model the spline knots are the nodes in the finite element mesh, but not all nodes are load control points. Then the equilibrium condition in Equation (12) for all the control points is

$$\mathbf{Z}\,\mathbf{y} = 0 \qquad \ldots (24)$$

where p is the total number of control points, $\mathbf{Z}$ is a $3 \times (2p)$ matrix and $\mathbf{y}$ is a $(2p) \times 1$ vector. The elements of the matrix $\mathbf{Z}$ are calculated with Equations (16) to (21) and are disposed in a matrix as in the following equation:

$$\mathbf{Z} = \begin{bmatrix} I_1 + J_1 & 0 & .... & I_i + J_i & 0 & .... \\ 0 & I_1 + J_1 & .... & 0 & I_i + J_i & .... \\ -(N_1 + O_1) & T_1 + U_1 & .... & -(N_i + O_i) & T_i + U_i & .... \\ \end{bmatrix} \qquad \ldots (25)$$

$$\begin{bmatrix} I_p + J_p & 0 \\ 0 & I_p + J_p \\ -(N_p + O_p) & T_p + U_p \end{bmatrix}$$

Vectors $\mathbf{x}$ and $\mathbf{y}$ are related by a $(2p) \times n$ matrix $\mathbf{\Psi}$.

$$\mathbf{\Psi x} = \mathbf{y}. \qquad \ldots (26)$$

Matrix $\mathbf{\Psi}$ is calculated with the weights given in Equations (7) and (8). If a point is a load control point, then its load components are in both vectors $\mathbf{x}$ and $\mathbf{y}$ and multiplying $\mathbf{x}$ by $\mathbf{\Psi}$ its load component remains. If the point is not a load control point, then its load components are related to the load components of the load control points as described by the weights.

If all the control points were load control points, matrix $\mathbf{\Psi}$ would be the identity matrix and $\mathbf{G}$ is $\mathbf{Z}$. $\mathbf{G}$ is evaluated by the multiplication of $\mathbf{Z}$ and $\mathbf{\Psi}$.

$$\mathbf{G} = \mathbf{Z\Psi}. \qquad \ldots (27)$$

In Fig. 9, there are seven load control points and no corners (a single spline is used). Therefore, if only normal loadings are considered $n = 7$ and $n = 14$ if both normal and transverse loadings are considered.

5.0 LINEARLY INDEPENDENT LOAD PARAMETERS

Assume that the loading parameters are stored in a vector $\mathbf{x}$ of dimension n such that $\mathbf{x} = \{R_1\ R_2\ \ldots\ R_n\}^T$. The goal is to find n vectors $\mathbf{x_i}$ that satisfy the equilibrium conditions, Equation (12), and represent the self-equilibrating loading configurations. The Lagrange multiplier method will be used to obtain vectors $\mathbf{x_i}$. For that purpose, define the $n \times 1$ unit vector $\mathbf{n}_i^T$ in which the ith term is equal to one.

Function e^* defined below is minimised subjected to the constraints in Equation (22).

$$e^* = \sum_{i=1}^{n} [(\mathbf{n}_i - \mathbf{x}_i)^T (\mathbf{n}_i - \mathbf{x}_i) - 2\mathbf{x}_i^T \mathbf{G}^T \mu_i] \qquad \ldots (28)$$

where $\boldsymbol{\mu_i}$ denote vectors of Lagrange multipliers. The solution to the problem is obtained making the derivatives of e^* with respect to $\mathbf{x_i}$ and $\boldsymbol{\mu_i}$ vanish that leads to

$$\mathbf{x}_i = [\mathbf{I} - \mathbf{G}^T(\mathbf{GG}^T)^{-1}\mathbf{G}]\mathbf{n}_i. \qquad \ldots (29)$$

$\mathbf{GG^T}$ is singular if the rows of $\mathbf{G}$ are linearly dependent. In practical situations it does not happen since $\mathbf{G}$ represents the equilibrium of forces and moments. Matrix $[\mathbf{I} - \mathbf{G}^T(\mathbf{G}\ \mathbf{G}^T)^{-1}\mathbf{G}]$ is symmetric although singular. In order to show that, consider the eigenvalue problem:

$$[\mathbf{I} - \mathbf{G}^T(\mathbf{GG}^T)^{-1}\mathbf{G}]\mathbf{q} = \alpha\mathbf{q} \qquad \ldots (30)$$

Initially, assume that $\alpha \neq 0$. Pre-multiplication of Equation (30) by $\mathbf{G}$ leads to: $\alpha\mathbf{Gq} = \mathbf{0}$. However, since $\alpha \neq 0$, $\mathbf{Gq} = \mathbf{0}$. Thus, returning to Equation (30), $\mathbf{q} = \alpha\mathbf{q}$, that implies in $\alpha = 1$. Next, assume that $\alpha = 0$ and consider $\mathbf{q} = \mathbf{G}^T\mathbf{z}$, where z is an arbitrary vector of three components. $\mathbf{q} = \mathbf{G}^T\mathbf{z}$ automatically satisfies $[\mathbf{I} - \mathbf{G}^T(\mathbf{G}\ \mathbf{G}^T)^{-1}\mathbf{G}]\mathbf{q} = \mathbf{0}$ what shows that any vector of the form $\mathbf{G}^T\mathbf{z}$ is an eigenvector to the problem and has a zero eigenvalue associated. Therefore, 1 is an eigenvalue of multiplicity $n - 3$ of matrix $[\mathbf{I} - \mathbf{G}^T(\mathbf{G}\ \mathbf{G}^T)^{-1}\mathbf{G}]$ whereas 0 is an eigenvalue of multiplicity 3. In practical applications the $n - 3$ eigenvectors with eigenvalue 1 associated are the basis vectors. The remaining three eigenvectors may be discarded since they correspond to linear combinations of the other $n - 3$.

6.0 RIB EXAMPLE

The ribs investigated in this work are simply supported along the edges with a 0·5 mm thick base plate, as defined in Fig. 4. The material of the rib is isotropic with Young modulus of 208·0GPa and Poisson ratio of 0·30. The elements used in the meshes of the ribs are biquadratic Lagrangian. The elements of the reinforcements are quadratic Timoshenko beams.

Figure 10 presents the shape of the rib investigated (dimensions in millimeters). The rib has four holes and panel reinforcements between each hole as illustrated in Fig. 10(a). The finite element mesh is divided into 6×40 elements. The panels are numbered as in Fig. 10(b). The basis piecewise linear loading functions are defined at the black dots in Fig 10(b), that is, the vertices of the plate and at the ends of the panels. Therefore, 25 different independent loading configurations result, since there are 14 load control points, considering that there are two coinciding load control points at each corner and that three eigenvectors are linearly dependent as shown in the previous section ($14 \times 2 - 3 = 25$). In Fig. 10(a), the three heavy dark lines are the panel reinforcements. The first reinforcement is located in between the first and second panels, the second reinforcement is in between the second and the third panels and the third reinforcement is between the third and fourth panels. Table 1 shows the optimal thicknesses of the rib panels and the optimal associated buckling loads. The cross section of reinforcements are rectangular and its dimensions (width and height) must be between 2·0 and 20·0mm. Table 2 presents the optimal dimensions of the three panel reinforcements.

The normalisation of the buckling loads is made with respect to the buckling loads of the design optimised against that loading distribution only. Therefore, the maximum normalised load for each design is obviously the one subjected to the loading configurations to which it was optimised, which is exactly 1·0. That does not happen for the design optimised for all loading distribution. Table 3 presents statistical results for the rib optimised where the maximum normalised load shown in the second column corresponds, in fact, to the second highest buckling load. The loading configuration to which the design is subjected in the minimum and maximum normalised load is presented between parentheses at the right of the load in Table 3.

The point to remark in Table 3 is that the minimum (worst) buckling load associated with the minimax optimal design (0·406) is always well above the worst buckling load associated with traditional designs where the loading has been kept fixed. Interesting is also the fact that the standard deviation of the minimax design is the lowest among all, meaning that it is able to efficiently withstand a variety of loadings. The worst loading is observed to be load case 8. However, when one takes load case 8 and fixes it the resulting optimal design (design 8) performs badly against load case 18. This serves to illustrate that ignoring load cases in the optimisation can have serious deleterious effects.

https://doi.org/10.1017/S0001924000000944 Published online by Cambridge University Press

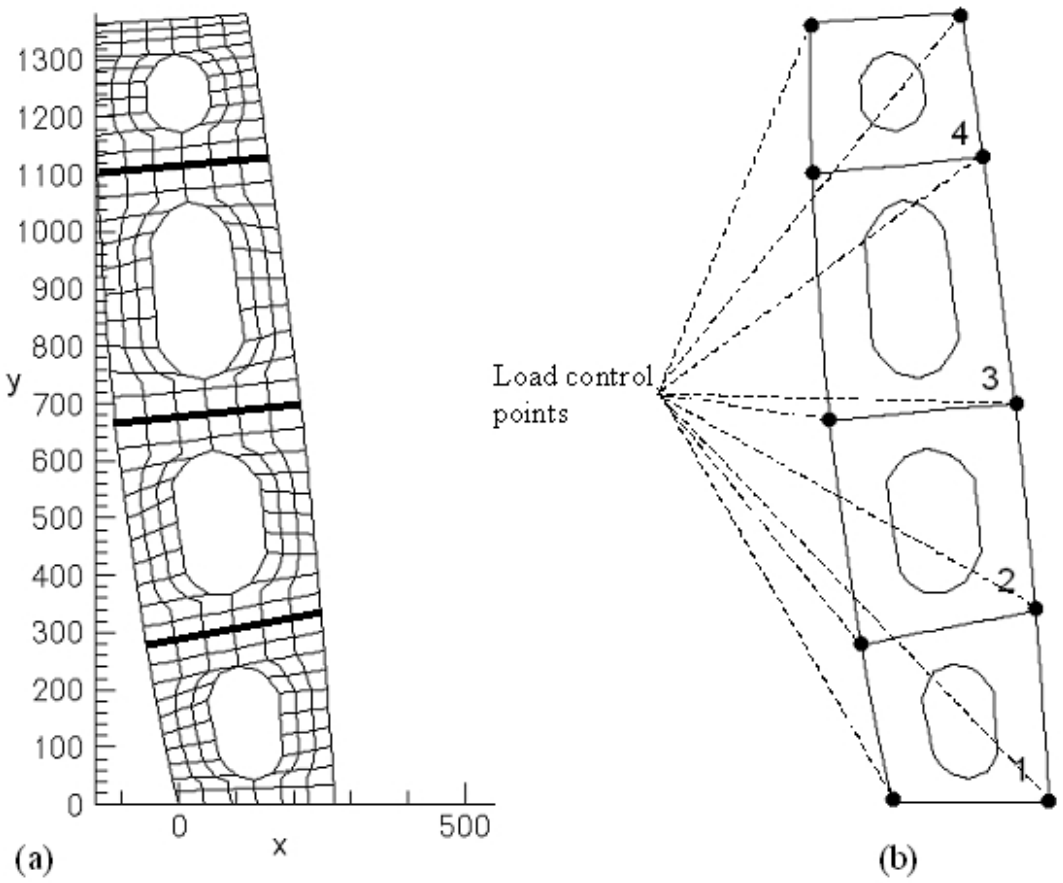

Figure 10. Rib with four holes.

Table 1
Optimal buckling loads and panel thicknesses

design	λ (N/m)	t_1 (mm)	t_2 (mm)	t_3 (mm)	t_4 (mm)
minimax	—	0·56	0·44	0·51	0·45
1	13,378	0·13	0·79	0·74	0·07
2	19,300	0·19	0·62	0·87	0·07
3	35,009	0·90	0·62	0·42	0·00
4	22,044	0·30	0·76	0·62	0·15
5	28,625	0·14	0·54	0·69	0·55
6	37,008	0·08	0·46	0·79	0·56
7	24,678	0·17	0·55	0·62	0·60
8	49,397	0·10	0·39	0·65	0·86
9	28,482	0·19	0·48	0·69	0·48
10	20,667	0·41	0·90	0·46	0·00
11	21,306	0·12	0·81	0·74	0·12
12	30,392	0·54	0·60	0·58	0·10
13	24,789	0·68	0·54	0·60	0·07
14	20,082	0·46	0·42	0·94	0·34
15	20,400	0·19	0·66	0·83	0·09
16	12,915	0·16	0·66	0·74	0·10
17	20,703	0·27	0·53	0·80	0·20
18	47,951	0·92	0·59	0·44	0·00
19	37,199	0·06	0·45	0·67	0·81
20	36,645	0·60	0·69	0·52	0·03
21	25,442	0·63	0·72	0·52	0·00
22	24,542	0·76	0·64	0·39	0·03
23	31,568	0·08	0·43	0·78	0·56
24	23,463	0·64	0·61	0·51	0·04
25	25,939	0·17	0·56	0·64	0·55

Table 2
Optimal panel reinforcement thicknesses (*h*) and widths (*d*)

design	h_1 (mm)	d_1 (mm)	h_2 (mm)	d_2 (mm)	h_3 (mm)	d_3 (mm)
minimax	2·62	2·02	2·03	2·02	2·03	5·24
1	2·23	2·59	3·06	2·30	5·20	2·02
2	4·11	2·00	2·01	2·01	2·01	2·01
3	2·00	2·00	2·01	2·01	2·24	2·02
4	3·09	3·02	2·00	2·02	2·03	2·03
5	2·00	2·00	2·00	2·01	2·02	2·11
6	2·94	2·01	2·02	2·02	2·01	2·02
7	3·39	2·23	2·01	2·01	2·00	2·01
8	2·01	2·02	2·59	2·17	2·41	2·02
9	3·15	2·02	2·02	2·02	6·24	3·40
10	4·58	5·00	2·03	2·01	2·02	2·02
11	2·02	2·02	2·02	2·01	2·00	2·01
12	10·06	2·02	2·02	2·02	2·02	2·02
13	2·18	2·00	2·02	2·02	2·00	2·02
14	3·62	2·00	2·02	2·02	4·75	4·35
15	3·22	2·50	2·00	2·00	2·02	2·02
16	9·79	2·52	2·84	2·95	4·17	3·13
17	4·03	2·02	2·02	2·02	4·07	2·55
18	2·02	2·02	2·02	2·02	2·02	2·02
19	2·66	2·21	2·00	2·01	2·00	2·01
20	6·41	2·02	2·01	2·01	2·01	2·01
21	2·01	2·01	2·01	2·01	2·35	2·09
22	9·56	2·00	9·02	2·00	2·00	2·01
23	5·40	2·28	2·02	2·27	4·79	2·01
24	3·85	5·11	2·00	2·00	6·18	2·14
25	2·90	2·02	2·02	2·02	2·02	2·02

https://doi.org/10.1017/S0001924000000944 Published online by Cambridge University Press

Table 3
Extremal and statistical results

design	minimum load	maximum load	average load	standard deviation
minimax	0·406 (11)	0·740 (13)	0·540	0·105
1	0·099 (18)	0·838 (11)	0·369	0·263
2	0·098 (8)	0·964 (1)	0·408	0·284
3	0·070 (8)	0·985 (18)	0·433	0·276
4	0·141 (8)	0·791 (11)	0·450	0·219
5	0·107 (18)	0·934 (6)	0·545	0·276
6	0·078 (18)	0·937 (23)	0·476	0·261
7	0·118 (18)	0·961 (25)	0·555	0·259
8	0·088 (18)	0·967 (19)	0·466	0·263
9	0·130 (18)	0·968 (5)	0·548	0·253
10	0·070 (8)	0·896 (22)	0·402	0·250
11	0·095 (18)	0·944 (1)	0·380	0·261
12	0·117 (8)	0·898 (24)	0·523	0·256
13	0·101 (8)	0·877 (24)	0·503	0·255
14	0·066 (18)	0·643 (9)	0·391	0·225
15	0·108 (8)	0·977 (1)	0·420	0·287
16	0·114 (18)	0·987 (1)	0·411	0·270
17	0·174 (8)	0·844 (2)	0·473	0·217
18	0·070 (8)	0·921 (3)	0·435	0·270
19	0·069 (18)	0·892 (8)	0·459	0·270
20	0·080 (8)	0·933 (21)	0·495	0·291
21	0·070 (8)	0·922 (20)	0·458	0·270
22	0·079 (8)	0·929 (3)	0·433	0·272
23	0·078 (18)	0·924 (6)	0·482	0·262
24	0·087 (8)	0·839 (12)	0·497	0·267
25	0·117 (18)	0·931 (5)	0·554	0·262

The proposed approach optimises the structural performance of the component for the load space defined by the load control points. Closely spaced load control points enrich the load space but may introduce loads that are unlike to occur in practical problems. Therefore, the choice of the load control points should be consistent with the expected load distribution transferred to the rib. Naturally, this loading distribution depends on structural details of the rib. For example, highly localised loads should be associated to the existence of a concentrated load applied to a fixation point. This would be the case of the support points of the landing gear.

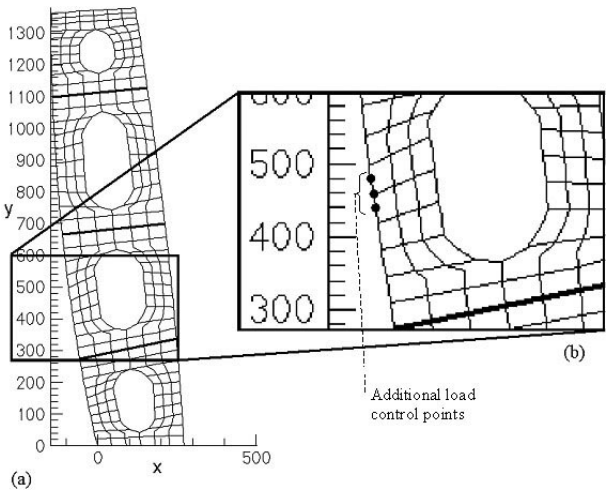

Figure 11. Rib with four holes and concentrated load.

Table 4
Optimal buckling loads and panel thicknesses: rib with concentrated load

design	λ (N/m)	t_1 (mm)	t_2 (mm)	t_3 (mm)	t_4 (mm)
minimax	—	0·47	0·50	0·47	0·44
1	21,403	0·01	0·38	0·92	0·33
2	22,853	0·27	0·59	0·74	0·22
3	41,098	0·12	0·37	0·68	0·81
4	27,698	0·12	0·51	0·68	0·57
5	44,055	0·89	0·58	0·45	0·02
6	18,403	0·21	0·63	0·85	0·04
7	50,390	0·12	0·40	0·63	0·86
8	30,814	0·16	0·44	0·76	0·55
9	25,556	0·67	0·54	0·61	0·09
10	21,095	0·42	0·85	0·49	0·00
11	15,466	0·21	0·58	0·80	0·05
12	24,402	0·15	0·57	0·61	0·60
13	40,462	0·28	0·99	0·50	0·00
14	21,824	0·35	1·08	0·38	0·00
15	58,211	0·46	0·96	0·37	0·00
16	28,611	0·67	0·71	0·40	0·08
17	26,086	0·21	0·80	0·68	0·10
18	64,011	0·12	0·81	0·73	0·12
19	36,861	0·87	0·64	0·43	0·00
20	64,051	0·22	0·61	0·81	0·17
21	29,183	0·67	0·55	0·54	0·10
22	39389	0·11	0·49	0·72	0·61
23	25,381	0·68	0·57	0·54	0·07
24	22,785	0·33	0·74	0·59	0·14
25	25,587	0·16	0·59	0·62	0·56
26	29,707	0·14	0·52	0·69	0·51
27	30,439	0·16	0·78	0·73	0·13
28	21,198	0·21	0·67	0·82	0·06
29	33,621	0·57	0·71	0·53	0·03
30	14,085	0·21	0·67	0·78	0·09
31	25,513	0·65	0·72	0·50	0·00

In order to illustrate the ability of the present approach to deal with these situations three additional load control points are considered in the rib model shown in Fig. 10. These additional load control points are three successive nodes on the rib boundary at the left side of the second hole. In Fig. 11, these nodes are highlighted with dark circles. Tables 4 and 5 present the dimensions of the panels and reinforcements and Table 6 presents extremal and statistical data regarding the optimisation process.

When three additional load control points are used to represent a concentrated load (Fig. 11, dimensions in millimeters), all panels become thicker but the thickness of the four reinforcements do not change significantly. This can be observed by comparing the dimensions in Tables 1 and 2 with Tables 4 and 5, respectively.

From Table 2 or Table 4 it can be inferred that the reinforcement dimensions were optimised to be close to the minimum possible in most cases for the rib with four holes. Most of the rib mass in these optimisations was arranged as reinforcement in the panels. It happened because the plate fails usually on the border of the holes. One of such buckling modes is shown in Fig. 12, obtained using the present code and a coarse mesh (Fig. 12(a)), the present code and a fine mesh (Fig. 12(b)), and MSC.Nastran and a fine mesh (Fig. 12(c)).

https://doi.org/10.1017/S0001924000000944 Published online by Cambridge University Press

Table 5
Optimal panel reinforcement thicknesses (h) and widths (d): rib with concentrated load

design	h_1(mm)	d_1(mm)	h_2(mm)	d_2(mm)	h_3(mm)	d_3(mm)
minimax	3·89	2·77	3·62	2·18	2·19	10·23
1	3·95	2·32	3·87	3·94	4·47	8·01
2	2·12	2·08	2·01	2·01	3·13	2·22
3	2·35	2·03	2·02	2·50	2·00	3·06
4	3·26	2·00	2·01	2·01	2·60	5·57
5	2·01	2·01	2·01	2·02	2·02	2·01
6	6·92	2·01	2·02	2·01	2·01	2·01
7	2·36	2·04	2·04	2·00	2·02	2·18
8	2·23	2·09	2·02	2·02	2·02	2·02
9	2·00	2·00	2·00	2·01	2·04	2·01
10	5·15	4·08	2·02	2·00	2·00	2·00
11	5·54	3·94	3·99	3·36	6·70	2·02
12	5·20	2·02	2·02	2·02	2·02	2·02
13	4·24	2·00	3·27	2·01	2·01	2·02
14	3·92	2·01	2·00	2·01	2·01	2·01
15	6·47	3·29	2·01	2·01	2·01	2·01
16	4·00	4·56	2·02	2·02	2·02	2·02
17	2·01	2·01	2·01	2·02	2·76	2·02
18	2·02	2·02	2·02	2·02	2·02	2·02
19	2·01	2·01	2·01	2·01	2·00	2·01
20	2·68	2·00	2·02	2·02	2·02	2·02
21	3·30	4·83	2·02	2·02	2·02	2·02
22	2·02	2·02	2·02	2·02	2·02	2·02
23	4·23	2·00	2·00	2·01	6·21	2·00
24	4·99	2·00	2·01	2·01	4·46	2·66
25	2·70	2·19	2·01	2·00	2·01	2·02
26	3·44	2·73	2·02	2·02	3·12	3·27
27	2·08	2·04	2·04	2·04	2·04	2·04
28	2·00	2·01	2·05	2·01	4·01	2·01
29	3·66	2·04	2·01	2·01	3·34	2·42
30	2·85	2·01	4·57	2·00	4·30	2·09
31	2·02	2·02	2·02	2·02	2·02	3·77

Table 6
Extremal and statistical results: rib with concentrated load

design	minimum load	maximum load	average load	standard deviation
minimax	0·386 (1)	0·742 (21)	0·517	0·101
1	0·059 (5)	0·593 (8)	0·342	0·198
2	0·191 (7)	0·900 (20)	0·504	0·218
3	0·103 (5)	0·911 (7)	0·439	0·235
4	0·105 (5)	0·913 (26)	0·520	0·253
5	0·073 (3)	0·868 (19)	0·453	0·242
6	0·084 (3)	0·911 (28)	0·442	0·259
7	0·104 (5)	0·907 (3)	0·458	0·240
8	0·123 (5)	0·905 (22)	0·494	0·239
9	0·108 (3)	0·895 (23)	0·510	0·228
10	0·067 (3)	0·836 (15)	0·461	0·254
11	0·088 (3)	0·947 (6)	0·439	0·257
12	0·119 (5)	0·966 (25)	0·538	0·235
13	0·067 (3)	0·815 (14)	0·400	0·223
14	0·067 (3)	0·800 (15)	0·389	0·232
15	0·067 (3)	0·919 (14)	0·409	0·245
16	0·103 (3)	0·776 (31)	0·460	0·227
17	0·111 (3)	0·908 (18)	0·467	0·260
18	0·106 (5)	0·870 (27)	0·417	0·250
19	0·067 (3)	0·924 (5)	0·445	0·251
20	0·152 (3)	0·970 (30)	0·489	0·262
21	0·113 (3)	0·976 (23)	0·514	0·230
22	0·098 (5)	0·926 (8)	0·497	0·255
23	0·097 (3)	0·977 (21)	0·519	0·240
24	0·134 (3)	0·843 (17)	0·511	0·212
25	0·125 (5)	0·950 (12)	0·541	0·237
26	0·117 (5)	0·926 (4)	0·538	0·251
27	0·123 (5)	0·955 (18)	0·457	0·272
28	0·093 (3)	0·945 (6)	0·449	0·275
29	0·077 (3)	0·953 (31)	0·509	0·255
30	0·106 (3)	0·954 (11)	0·469	0·277
31	0·067 (3)	0·836 (29)	0·472	0·243

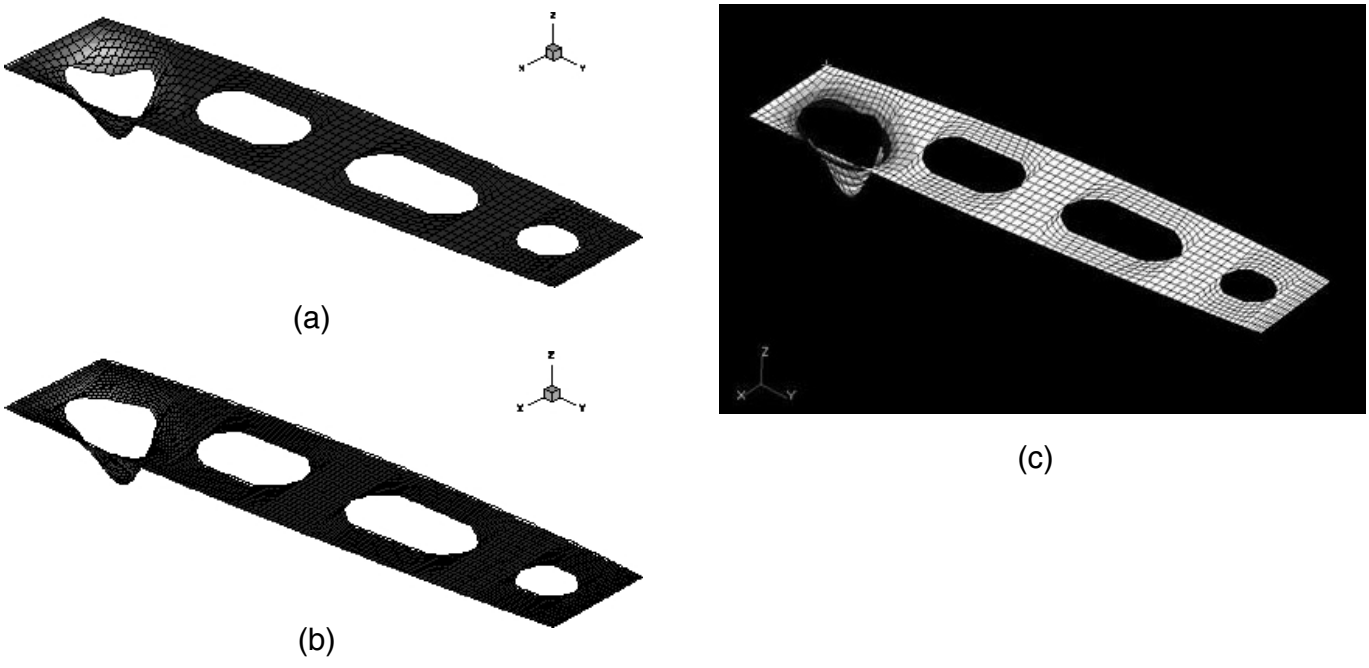

Figure 12. Buckling mode.

https://doi.org/10.1017/S0001924000000944 Published online by Cambridge University Press

7.0 CONCLUSIONS

The new procedure proposed is applied to isotropic plates with different shapes. The buckling optimisation takes the variability of the loading distribution into account. All independent self-equilibrating loading distributions represented by piecewise linear functions are investigated as possible loading cases with equal chance of occurring. As a result, when compared to the designs for fixed loading distributions, the resulting optimal design was proved to be insensitive to perturbations in the loading distributions within the admissible load set. This conclusion is possible by the observation of Tables 3 and 6. The resulting optimal design presents the lowest population standard deviation in all analysed plates. The design optimised for all load configurations will perform well under all possible loading configurations. The other designs perform very well or very poorly depending on the loading configuration.

Three additional load control points are defined in the rib with four holes in order to simulate the effect of a concentrated load. The admissible load space is larger; there are six more independent loading distributions. The resulting optimal design yields lower average normalised buckling load and lower standard deviation than the rib without these additional load control points. The panels of the resulting optimal design in become thicker when concentrated loads are present.

ACKNOWLEDGEMENTS

This work was partially financed by the Brazilian agency CNPq (grants no 304642/2003-7 and no 302112/2003-0).

REFERENCES

1. CHAO, C.C., KOH, S.L. and SUN, C.T. Optimization of buckling and yield strengths of laminated composites, *AIAA J*, 1975, **13**, (9), pp 1131-1132.
2. HIRANO, Y. Optimum design of laminated plates under axial compression, *AIAA J*, 1979, **17**, (9), pp 1017-1019.
3. HAFTKA, R.T. and WALSH, J.L. Stacking sequence optimization for buckling of laminated plates by integer programming, *AIAA J*, 1992, **30**, (3), pp 814-819.
4. FOLDAGER, J.P. Design of Composite Structures 1999, PhD thesis, Aalborg University, Institute of Mechanical Engineering, Denmark.
5. MIKI, M. and SUGIYAMA, Y. Optimum design of laminated composite plates using lamination parameters, *AIAA J*, 1993, **31**, (5), pp 921-922.
6. SUN, G. and HANSEN, J.S. Optimal design of laminated-composite circular-cylindrical shells subjected to combined loads, *J Applied Mechanics*, 1988, **55**, (3), pp 136-142.
7. BRUHN, E.F. *Analysis and Design of Flight Vehicle Structures*, 1973, Tri-State Offset, Cincinnati, OH.
8. NIU, M.C.Y. *Airframe Stress Analysis and Sizing*, 2001, Hong Kong Conmilit Press, Hong Kong.
9. DE FARIA, A.R. and HANSEN, J.S. On buckling optimization under uncertain loading combinations, *Structural and Multidisciplinary Optimization J*, 2001, **21**, (4), pp 272-282.
10. DE FARIA, A.R. and DE ALMEIDA, S.F.M. Buckling optimization of plates with variable thickness subjected to nonuniform uncertain loads, *Int J Solids and Structures*, 2003, **40**, (15), pp 3955-3966.
11. DE FARIA, A.R. and DE ALMEIDA, S.F.M. Buckling optimization of variable thickness composite plates subjected to nonuniform loads, *AIAA J*, 2004, **42**, (2), pp 228-231.
12. POWELL, M.J.D. An efficient method for finding the minimum of a function of several variables without calculating derivatives, *Computers J*, 1964, **7**, pp 155-162.
13. GERALD, C.F. and WHEATLEY, P.O. *Applied Numerical Analysis*, 1985, Addison-Wesley Publishing.